Unraveling the role of ultrasound in hydrothermal interzeolite conversion using a tubular ultrasound-integrated reactor

Elena Brozzi,[†] Michiel Dusselier,[‡] and Simon Kuhn[*,†]

†*KU Leuven, Department of Chemical Engineering, Celestijnenlaan 200F, 3001 Leuven, Belgium*

‡*KU Leuven, Center for Sustainable Catalysis and Engineering, Celestijnenlaan 200F, 3001 Leuven, Belgium*

E-mail: simon.kuhn@kuleuven.be

Supporting Information

S(I): Zeolite characterization and reference material

X-ray powder diffraction (PXRD) was performed on the as-made samples on a high-throughput STOE STADI P Combi diffractometer in transmission mode with focusing Ge(111) monochromatic X-ray inlet beams (λ = 1.5406 Å, Cu Kα source) to picture the mother and daughter zeolite crystallinity evolution over time. TGA curves are obtained using a Mettler Toledo TGA/DSC 3+ by subjecting the as-made samples to a flow of air with a temperature ramp of 10 °C/min, between 30 and 800 °C. Prior to further analysis, the as-made zeolite is subjected to calcination in stagnant air at 580 °C for 6 hours, reached with a heating ramp of 1 °C/min. Surface area and porosity are measured by N_2 physisorption (Tristar II 3020, Micromeritics) after degassing the samples for >5 hours at 300 °C. Si/Al ratio of the product is determined

via ICP-OES (Perkin Elmer Optima 8300). Prior to analysis, samples were dissolved by microwave digestion with hydrofluoric acid 40 wt%. Scanning Electron Microscopy (SEM) images are taken with JEOL JSM-6010LA and analysed manually with ImageJ[1] to extract the particle diameter. Only particles with fully visible circumference were analysed and the longest dimension was measured and considered as "raw particle diameter". The number crystal size distribution (CSD) is calculated using MATLAB from these raw particle diameter data with a bin size of 100 nm.

Figure S1a contains the reference crystalline patterns of the commercial FAU used in this work, and MFI reference pattern obtained from the IZA website[2], while Figure S1b compares the crystallinity of the mother zeolite before synthesis, after being pretreated for 10 min in an ultrasonic bath at maximum power (120 W, VWR USC-THD, 45 kHz), or under 10 min stirring. It is possible to see that no major differences between the two patterns arise, proving that ultrasonic pretreatment helps de-agglomeration of FAU without affecting the dissolution stage, which only occurs during the hydrothermal treatment. Figure S2 shows the morphology and size of the commercial FAU used in this work.

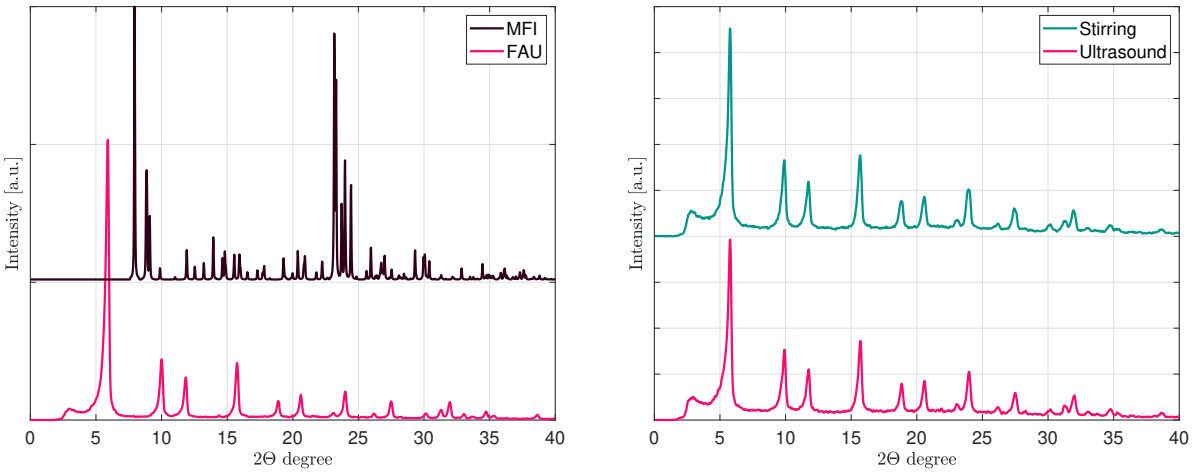

(a) (b)

Figure S1: PXRD patterns of a) commercial FAU385 used for all the experiments, and TPAOH-synthesized ZSM-5 (MFI framework) available on the International Zeolite Association website[2]; b) solids recovered from the suspension before synthesis after being pretreated for 10 min either with ultrasonic bath at maximum power, or stirring.

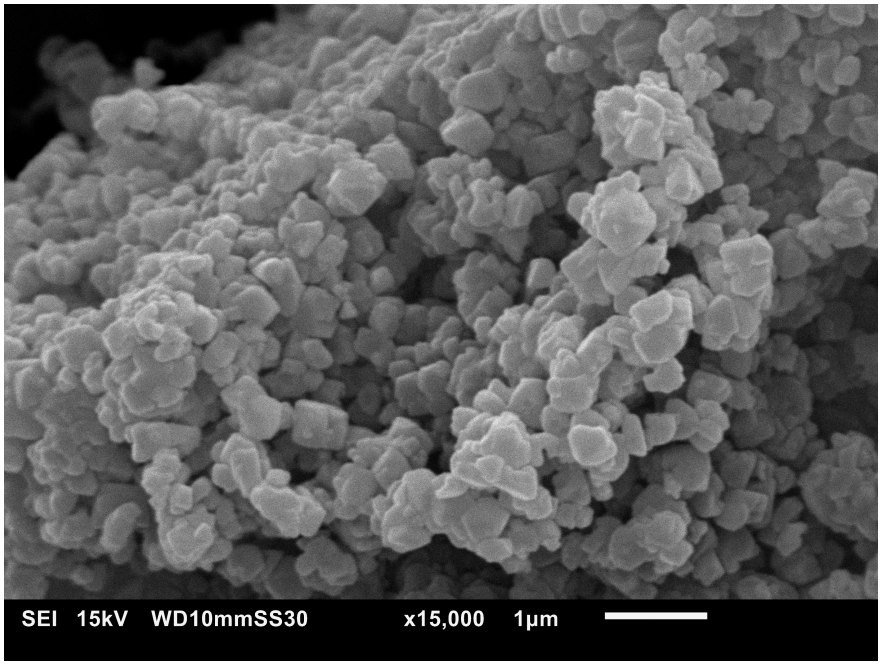

Figure S2: SEM image of commercial FAU (TOSOH HSZ390HUA) used for all the experiments.

S(II): Interzeolite conversion in different reactor setups

Figure S3 depicts the three reactor setups used in this work: a traditional Teflon-lined stainless steel autoclave of 23 mL, a custom-made U-shaped stainless steel tubular reactor (TR) of 5 mL, and the PTFE US-integrated coiled reactor (CR), with an internal volume of 12 mL, inserted into an aluminium box for temperature control. Table S1 summarises the main properties of the three systems. IZC in the autoclave suffers from well-known slow heating[3,4] if compared with the other two reactors due to the use of a convection oven as heat transfer method. However, the small volume of oil that can be recirculated in the aluminium box around the CR limits the heat transfer rate. This is also evident from the drop in temperature between 10 and 15 min in each curve in Figure S5, since even the injection of the suspension at ambient temperature affects the temperature control during the first minutes of the synthesis. Mainly for this reason, and for the use of different materials in the CR and in the TR, there is a difference in the crystallization rate between the reactors, despite the much higher S/V in the case of the CR.

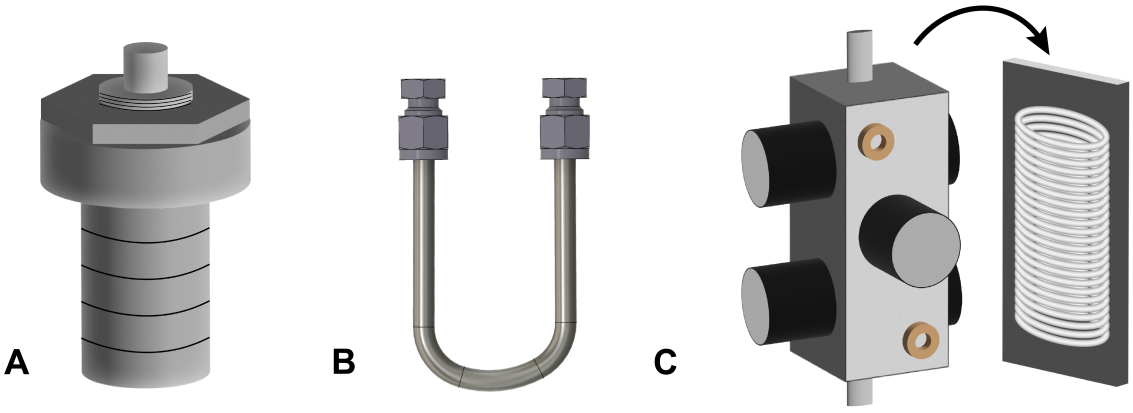

Figure S3: Types of reactors used in this work: A) Teflon-lined stainless steel autoclave, B) U-shaped stainless steel tubular reactor, C) Coiled PTFE tubular reactor.

Table S1: Comparison of geometrical and process parameters among the three types of reactors investigated in this work for FAU to MFI IZC. S/V = surface to volume ratio. ** coiled reactor considered as an open cylinder. SS = stainless steel.

Type of reactor	**Autoclave**	**Tubular reactor**	**Coiled reactor**
Inner diameter [mm]	N.A.	4.57	2
Outer diameter [mm]	N.A.	6.35	3
Volume [mL]	23	5	12
S/V [m^2/m^3]	1.4	8.8	2042**
Material	Teflon liner and SS	SS	PTFE
Heat transfer medium	Convection oven	Recirculating oil bath	Recirculating oil bath
Heat transfer medium volume	N.A.	3.5 L	140 mL
Type of mixing	Stirred	Static	Static
Cooling technique	Water bath	Ice bath	Quenching

Figure S4 shows the temperature profiles around the CR and inside the recirculating pump (oil bath) during a 20 min experiment under 240 W of sonication versus silent conditions. It can be seen from the different bath settings, represented by the dashed lines, that even at high temperatures, ultrasound is capable of dissipating some energy via heat. The temperature profiles of a selection of partial sonication experiments are depicted in Figure S5, where it is possible to discern the injection moment for all four curves (the sudden drop between 10 and 15 min). For the two partial sonication cases, the moment when ultrasound is turned on or off is also clearly visible from the temperature profile oscillation. When ultrasound is switched off, there is first a sudden rise in the oil temperature, which afterwards drops and has to be then controlled manually by adjusting the reservoir temperature. The opposite behaviour occurs when switching ultrasound on: first, a drop in temperature is detected, but once ultrasound starts dissipating heat, the oil bath temperature is adjusted to maintain a reactor temperature around 160±2 °C.

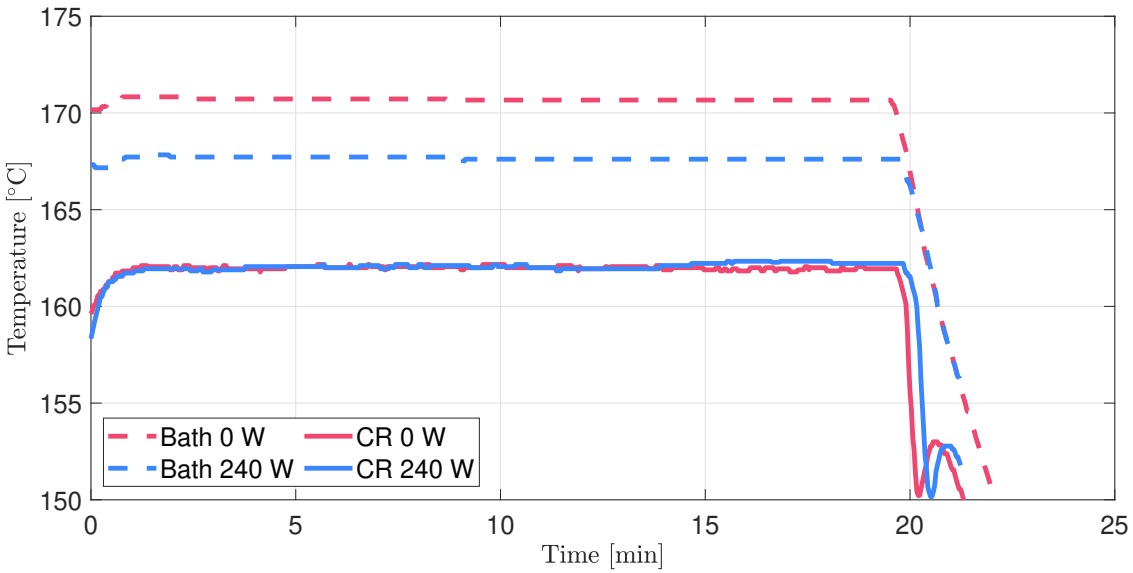

Figure S4: Comparison of the temperature profiles of the oil inside the reactor box and inside the recirculating pump during a 20 min experiment with or without ultrasonication.

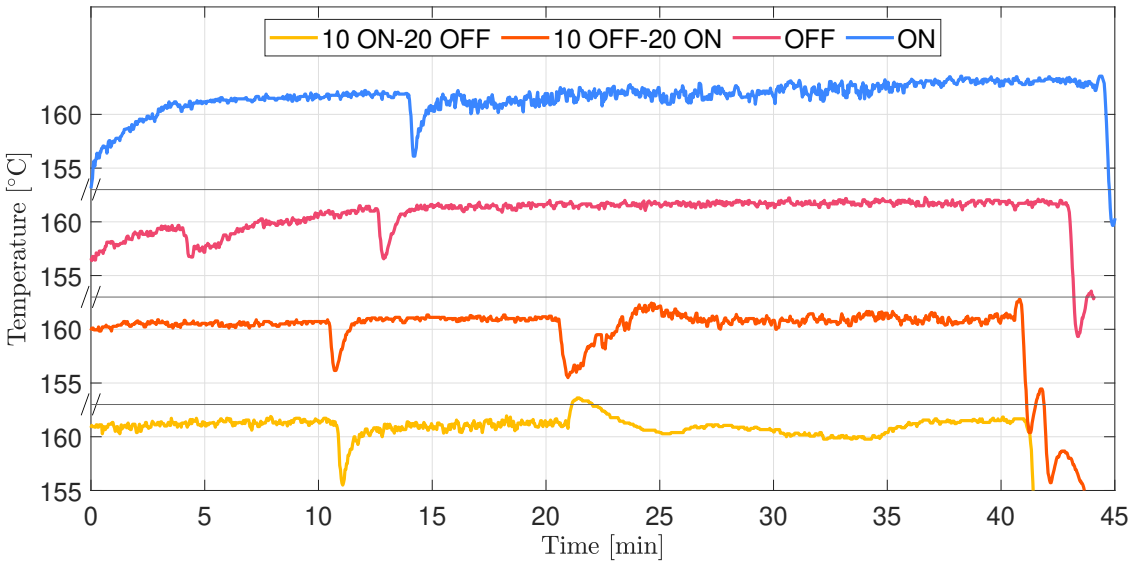

Figure S5: Comparison of the temperature profiles of the oil inside the reactor box for selected cases of the partial sonication experimental campaign. The drop between 10 and 15 min in each experiment represents the injection, or time 0, after which the reaction time starts to be counted. The oscillations between 20 and 25 min for the bottom two curves are linked to the shutting OFF or ON the ultrasonic device.

Comparison between silent and US-assisted IZC

Solid yield (SY) is determined by Equation S1, where the applied correction factor is based on the average weight loss of a dry sample obtained by TGA (about 11.5 wt%), which corresponds to the maximum incorporation of the TPA^+ in one MFI unit cell[5]. Every experimental point with error bars in Figure 2 is based on a minimum of three replicates.

$$\mathrm{SY} = \frac{\text{Sample weight}}{\text{Mass of FAU in the reactor}}(1 - 0.115) \tag{S1}$$

Table S2 contains the mean values and the error on the mean for the experiments conducted with a reaction time of 20, 30, and 45 min reaction time, either in US-aided or silent conditions. The t-test is performed considering the two as independent populations. The P-value obtained should be <0.05 to state that the two averages are *significantly* different from each other[6]. This is the case for the experiments at 20 and 30 min, while the difference at 45 min is not significant based on to the obtained P-value.

Table S2: Mean solid yield and error on the mean for silent and US-aided experiments at 20, 30, 45 min reaction time. All the errors are calculated based on 3 to 7 replicates.

Residence time	20 min	30 min	45 min
Average 0 W	11.2 ± 2.9	19.1 ± 12.1	40.1 ± 15.7
Average 240 W	16.7 ± 5.9	38.1 ± 6.6	51.2 ± 7.5
P-value	0.049	0.032	0.32

The incorporation of TPA cations in the MFI framework is depicted by the TGA curves in Figure S6a between 20 and 45 min, *i.e.*, the crucial synthesis times to have better understanding on the crystal growth under ultrasonication. The most striking difference in this case is the larger presence of water for the 20 min silent synthesis, followed by a substantial (around 3 wt%) amount of TPA^+ loosely attached to the framework, and therefore more prone to lower temperature combustion (100-280 °C)[7]. All the curves also show the typical shoulder around 350 °C, which is usually attributed to the presence of the cations at the channels intersection, to balance the formation of SiO^- defects in the framework[7,8]. A larger amount of occluded TPA^+ is found in the ultrasonicated samples within the first 30 min of reaction time, which can better stabilize the SiO^- defects in this high Si environment. As a result of this charge stabilization, a higher Si/Al ratio in the bulk is detected for the product synthesized with ultrasound, as shown in Figure S7. In accordance with Devos et al., the process is now in the III stage of IZC, where the Si/Al ratio increases along with the yield[9]. During this growth stage, it seems like ultrasound promotes Si incorporation in the framework, which explains the higher yield values compared to silent synthesis.

Another way to look at crystallinity is via N_2 physisorption, as the microporosity evolves with time until full crystallization is achieved. The stronger upwards tail present in Figure S8a, at 20 min and still slightly 30 min, can be either attributed to the presence of amorphous materials, or, as visible from PXRD patterns, to the persisting undissolved FAU crystals, which have a higher microporosity and present the same tail in their initial conditions. For this reason, samples before 20 min synthesis are not analyzed via physisorption. On the other hand, this tail is not present in ultrasonicated samples, which show a type I

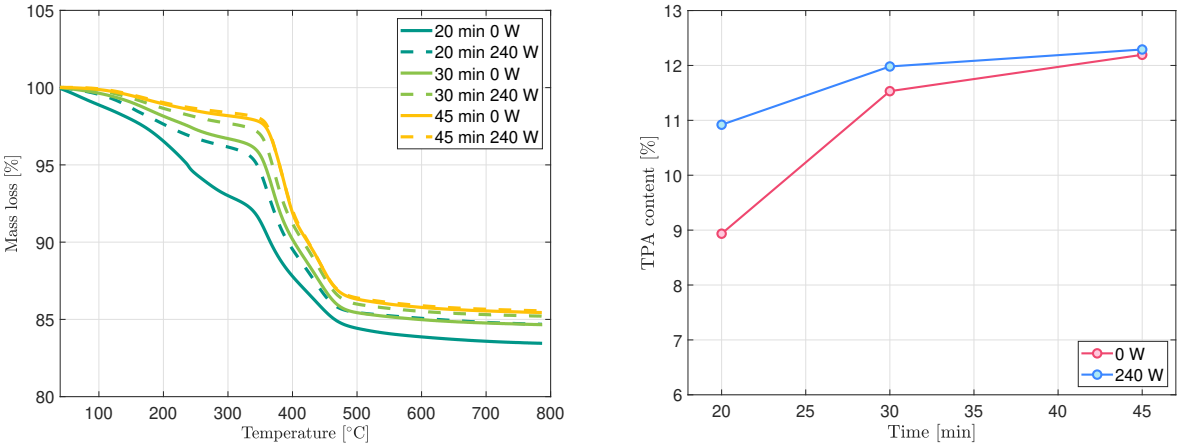

(a) (b)

Figure S6: a) Comparison of TGA curves for 20, 30, and 45 min synthesis in silent (0 W) and under ultrasonication (240 W); b) TPA^+ weight % occluded in the zeolite framework after 20, 30, and 45 min synthesis, calculated as wt% loss between 300 and 550 °C from TGA curves.

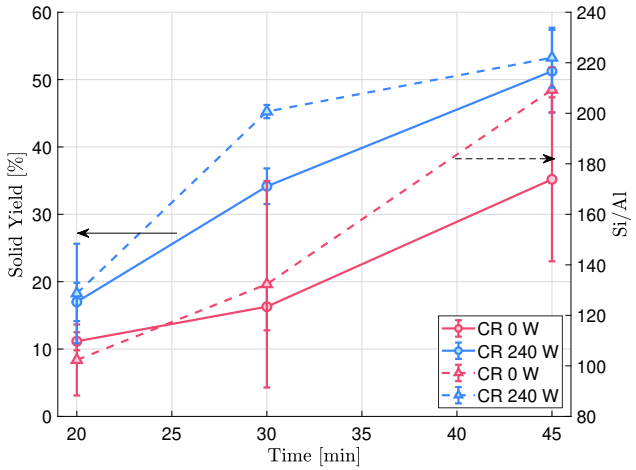

Figure S7: Yield (solid lines, left axis) and Si/Al ratio (dashed lines, right axis) trends in the IZC synthesis product between 20 and 45 min of synthesis time.

isotherm typical of microporous materials at all stages of crystal growth. There is no major difference between silent and US-assisted MFI in terms of microporosity and surface area.

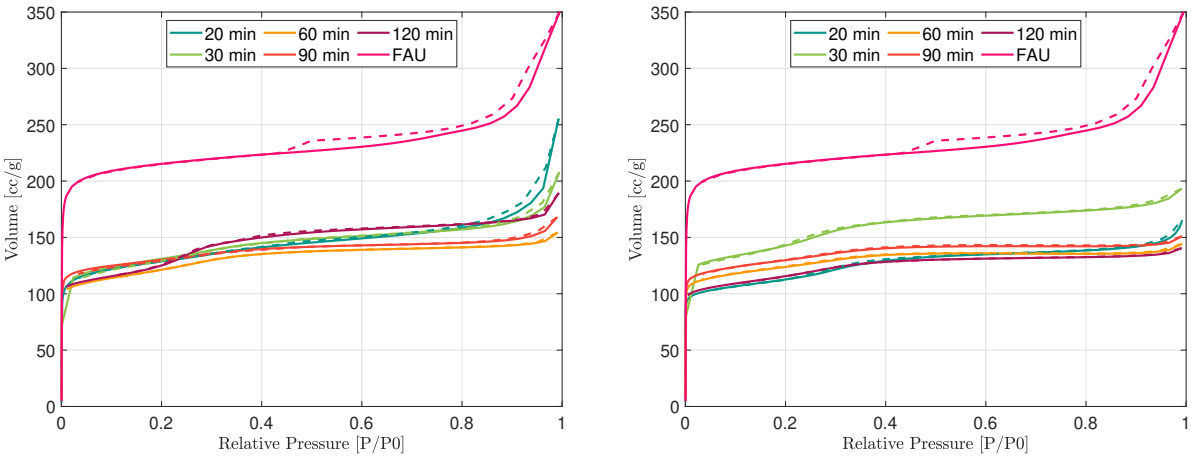

Figure S8: N_2 adsorption isotherms over time for MFI synthesized a) in silent conditions in the CR and b) under 240 W ultrasound for the entire reaction time. Both contain the physisorption curve of the commercial FAU used as mother zeolite in all IZC syntheses in this work.

The overall rate of the process can be evaluated by looking at the first derivative of the yield curve; a logistic model (sigmoidal curve) is used together with *lsqcurvefit* MATLAB solver to fit the experimental data. Figure S9a shows the experimental data as well as the fitting with its 95% confidence interval for both the silent and US-assisted synthesis cases. The first derivative is calculated based on the fitting curve using the finite difference method, and reported in Figure S9b.

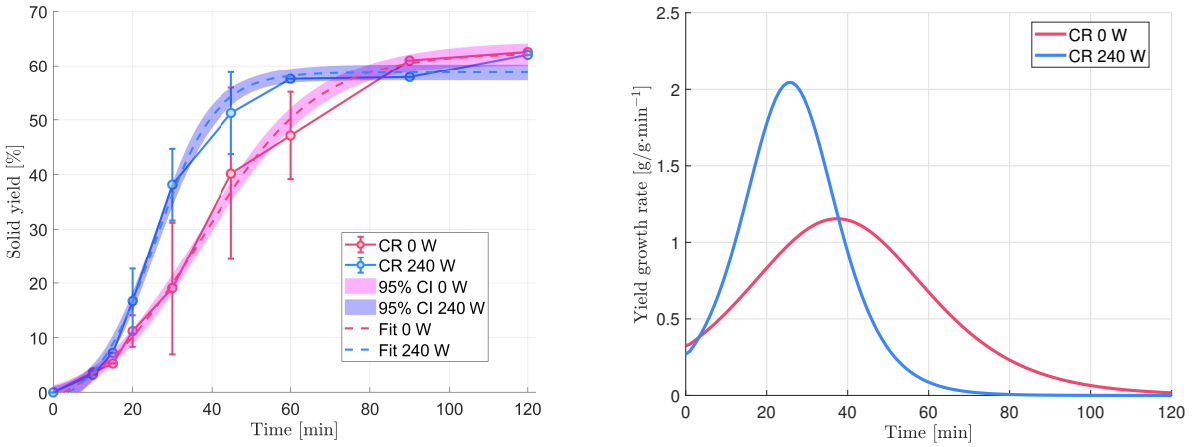

(a) (b)

Figure S9: a) Curve fitting on the experimental data for the yield curve of the coiled reactor in silent and US-mode of operation. The shaded area represents the 95% confidence interval. b) First derivative of the fitting of the TGA-corrected yield curve for silent and US-assisted synthesis.

S(III): Terephthalic acid dosimetry

Terephthalic Acid (TA) Dosimetry is carried out in the reactor system with the following reactant composition: 10 mM[10] TA (99+% Acros Organics) , a pH 7.5 phosphate buffer (2.5 mM NaH_2PO_4 - Merck Supelco Emsure ACS Reagent - and 7.5 mM K_2HPO_4 - Merck Emprove Expert), and 0.0217 mol/L of NaOH (anhydrous ≥98% pellets, Sigma Aldrich) to ensure a similar calculated final pH as in the work of Rajamma et al.[11]. ·OH radicals are produced in the system by two means: via ultrasonication, or via radical initiator, by adding 3.5 mM of sodium persulfate (SPS, ≥98%, Sigma Aldrich) to the TA solution. The experiments are performed by injecting the TA solution into the CR setup previously set to the desired temperature (and pressure) conditions, and let it react for 30 min. Collection of the solution is done by opening the connection between the end of the reactor tube and the ball valve. The first and last 2 millilitres of reacted solution are discarded, to ensure that the liquid is not diluted with unreacted solution present in the dead volume of the line.

The product is analysed via fluorescence spectroscopy (FLS980, Edinburgh Instruments), using a quartz cuvette (Hellma) with 10 mm optical path and a solution volume of 3 mL.

The spectra are recorded between 350 and 600 nm with a 1 nm step and 0.2 s dwell time, with an excitation wavelength of 312 nm. Slit width is fixed at 1 nm and 2 nm for ultrasonicated samples and for samples with SPS, respectively. All the curves are shown as relative fluorescence intensity as compared to the intensity obtained for 30 min sonication at 25 °C and 1 bar. Normalization of the data is done according to Equation S2, where p_i stands for the normalized data point x_i:

$$p_i = \frac{x_i - \min(x)}{\max(x) - \min(x)} \tag{S2}$$

HPLC analysis is conducted in a Shimadzu Prominence-i LC-2030C, using a 4.6x250 mm packed column Shim-pack GIST C18 5μm. HPCL grade Acetonitrile (AN) and 0.1% v/v H_3PO_4 in Milli-Q water are used as solvents with the following method: 0 min to 3.5 min, constant injection of 22% AN and 78% H_3PO_4 solution; from 3.5 min until 9 min linear increase of AN% until 80%, and kept constant until 10.5 min, then immediate switch to initial AN and H_3PO_4 % (22 and 78%, respectively) until the end of the run (13.5 min). Total injection volume of the solution: 5 μL. Figure S10a shows the HPLC chromatogram of the TA solution after being subjected to 30 min of ultrasonication at 160 °C and 6.5 bar (IZC synthesis conditions). The peak around 7 minutes can be attributed to TA itself and no other peaks are visible. On the other hand, interaction between TA and SPS at high temperature causes extensive TA oxidation, visible from the multitude of peaks appearing in Figure S10b, probably as a consequence of persulfate radicals formation and organic attack[12]. The US-assisted high-temperature dosimetry is repeated, which fluorescence spectra are depicted in Figure S11 and called S1 and S2, respectively. These solutions are then recycled for another round of dosimetry under radical-forming conditions (80 °C and with SPS). The recycled solution clearly shows the formation of 2-HTA (black curve in Figure S11). This check concludes that the two initial S1 and S2 solutions did not undergo any degradation nor oxidation during their first cycle of dosimetry, and could interact with radicals in the recycling round.

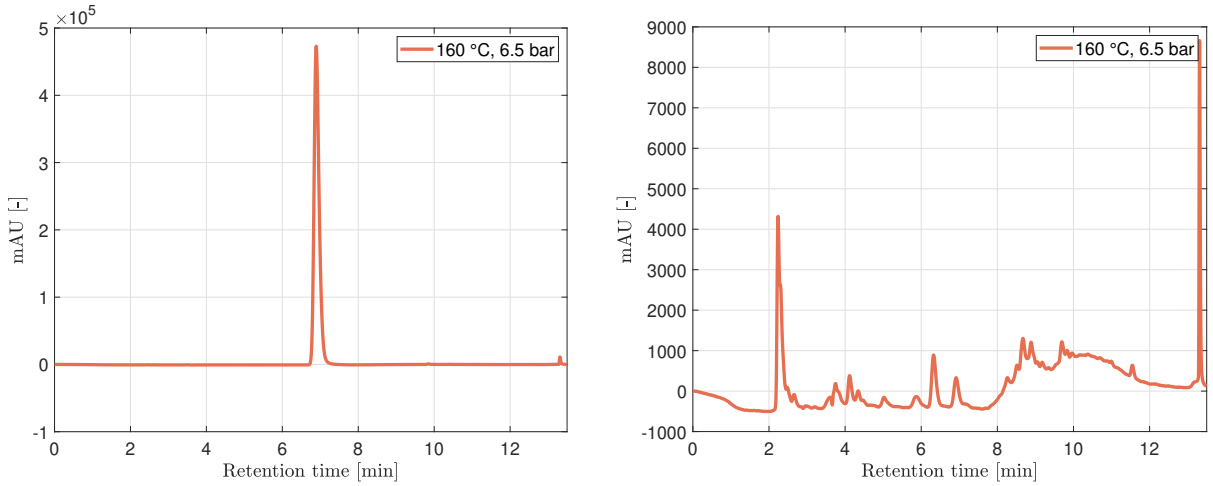

(a) (b)

Figure S10: HPLC chromatograms at 275 nm wavelength of the product solution after terephthalic acid dosimetry performed at 160 °C and 6.5 bar for 30 min, with a) ultrasound as radical source, or b) sodium persulfate as radical initiator.

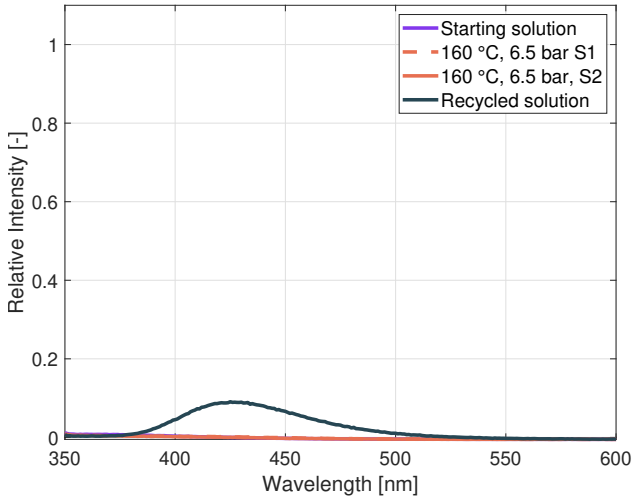

Figure S11: 2-HTA fluorescence spectra with excitation wavelength 312 nm. The curves show the effect of subjecting recycled TA solution (S1 and S2) after high temperature and pressure experiments under ultrasound, to a lower temperature treatment in presence of SPS to verify for formation of radicals and possible degradation of TA during the first dosimetry stage. All the curves have been normalized based on the intensity of the curve obtained from ultrasound-generated radicals at 25 °C and 1 bar.

S(IV): Low temperature synthesis

Method description

In order to ensure radical-bearing conditions from ultrasound, low temperature zeolite syntheses (LTS) are performed following an analogous procedure as the IZC hydrothermal syntheses. To find the adequate synthesis temperature that could achieve the highest radical formation without compromising the residence time, TA dosimetry at different temperatures (25-140 °C), pressures (1-4 bar), and ultrasonic power inputs (120-300 W) is performed. In this case, the results obtained from TA dosimetry were analysed with Horiba Fluorolog 3.22, with a slit width of 3.098 nm, excitation wavelength of 317 nm, emission spectrum between 350 and 600 nm, and a superimposition of 3 scans. Similarly, optimal ethanol (EtOH) concentration for scavenging effect[13,14] is investigated at 25 °C and ambient pressure, *i.e.*, the condition with the highest radical production according to dosimetry experiments, illustrated in Figure S13. Eventually, LTS experiments in presence of a radical scavenger are also performed. In this case, EtOH is added to the synthesis suspension right before the loading of the syringe (hence after ultrasonic dispersion of the FAU).

Results and discussion

FAU-to-MFI IZC is performed at a lower temperature of 90 °C to ensure the presence of radicals when ultrasound is applied, as visible from Figure S12a. 90 °C is chosen as the highest temperature that can produce a substantially detectable amount of radicals, even though by increasing the temperature, the intensity already decreases about 65%. An increase in input power to 300 W (25 W/mL) enhances radical formation but it can contribute to system instabilities when working for long hours as the transducers tend to heat up. Moreover, even a slight increase in pressure to 2 bar is enough to completely suppress radical formation, as clear from Figure S12b. It is chosen eventually to work with autogenous pressure and again 240 W (20 W/mL) input power. As a consequence of the lower temperature, the kinetics of

the interzeolite transformation is slowed down, therefore longer synthesis times (between 4 and 10 h for the CR, up to 24 h in the TR) are investigated.

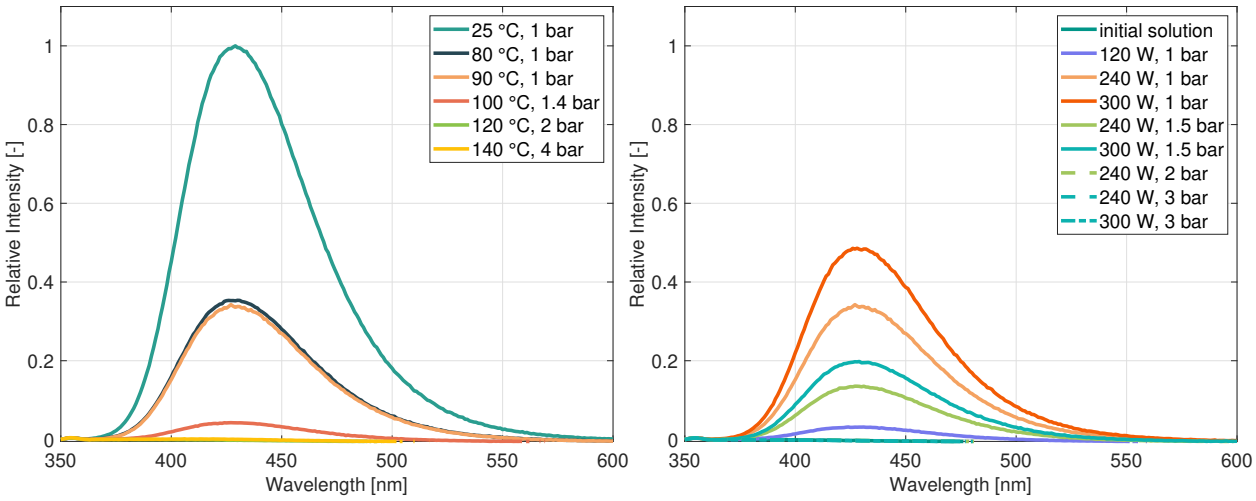

(a) (b)

Figure S12: Fluorescence spectra of 2-hydroxyterephthalic acid as a consequence of the interaction between terephthalic acid and ·OH radicals a) with 240 W sonication, at different system temperatures and and pressures, and b) at 90 °C, with different sonication power and system pressures. All the curves have been normalized based on the intensity of the curve obtained from ultrasound-generated radicals at 25 °C and 1 bar.

After 4 h of synthesis time, in the case of the tubular reactor (TR), again full amorphization occurs before any crystallization onset, as evident from the PXRD pattern in Figure S14a. MFI starts to form between 6 and 8 h, but a yield of 60% is achieved only after 24 h. Due to the impossibility of operating the CR for one day long, syntheses are performed up to 10 h. Again, in this case FAU dissolution process is slower than MFI crystallization, and the two processes overlap. Unexpectedly, at lower temperatures, the faster FAU dissolution rate in the TR compared to the CR is even more evident, although the faster heat transfer should be of lower impact at 90 °C than at 160 °C. Perhaps the reactor geometry, combined with slower diffusion at lower temperatures, causes a more difficult contact between the FAU and highly alkaline areas to enable dissolution.

A clear difference in crystallization kinetics is visible when comparing Figure S14b and Figure S14c: after 6 h under irradiation, MFI characteristic peaks are visible (together with

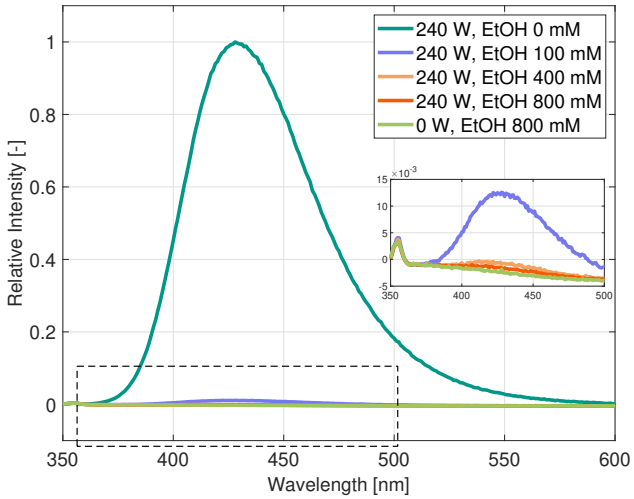

Figure S13: Fluorescence spectrum of 2-hydroxyterephthalic acid as a consequence of the reaction of terephthalic acid with ultrasound-generated radicals, and their suppression by ethanol at different concentrations. All the curves have been normalized based on the intensity of the curve obtained from ultrasound-generated radicals at 25 °C and 1 bar.

undissolved crystalline FAU), while in silent conditions only slight MFI reflections around θ=8° can be detected. From the evaluation of the yield in Figure S14d, there is not much difference in the amount of solid retrieved after 6 h synthesis. It is hypothesized that after partial dissolution, the remaining solid phase is involved in the FAU-to-MFI transformation, and this is enhanced by ultrasound. Moreover, there is also a visible effect on zeolite growth, since the solid yield at 8 h in the case of ultrasonication is substantially higher than in the CR silent or TR case. Overall, the MFI resulting from low temperature synthesis exhibits a crystal size <200 nm (Figure S15A and C), and the isotherms in Figure S16 show a microporous material with a hysteresis loop >0.8 $P/P0$, sign of condensation of N_2 in the inter-crystalline space[15] .

To give more insights into the underlying US-generated mechanism, the synthesis in the CR is performed with and without 800 mM of EtOH as a radical scavenger, which shows almost complete radicals suppression at 25 °C (Figure S13). A control experiment is also carried out by adding EtOH in silent conditions. In both cases, the total solid yield drops almost equally of 26 and 27 percentage points for the silent and ultrasonicated case, respectively. It is concluded that the addition of EtOH suppresses MFI crystallization in

general, as also visible from the SEM images in Figure S15, showing important presence of undissolved FAU, but it does not show any particular scavenging effect when added in combination with ultrasound. No additional elucidation of the underlying US-generated mechanisms affecting IZC in this setup can be given from LTS experiments.

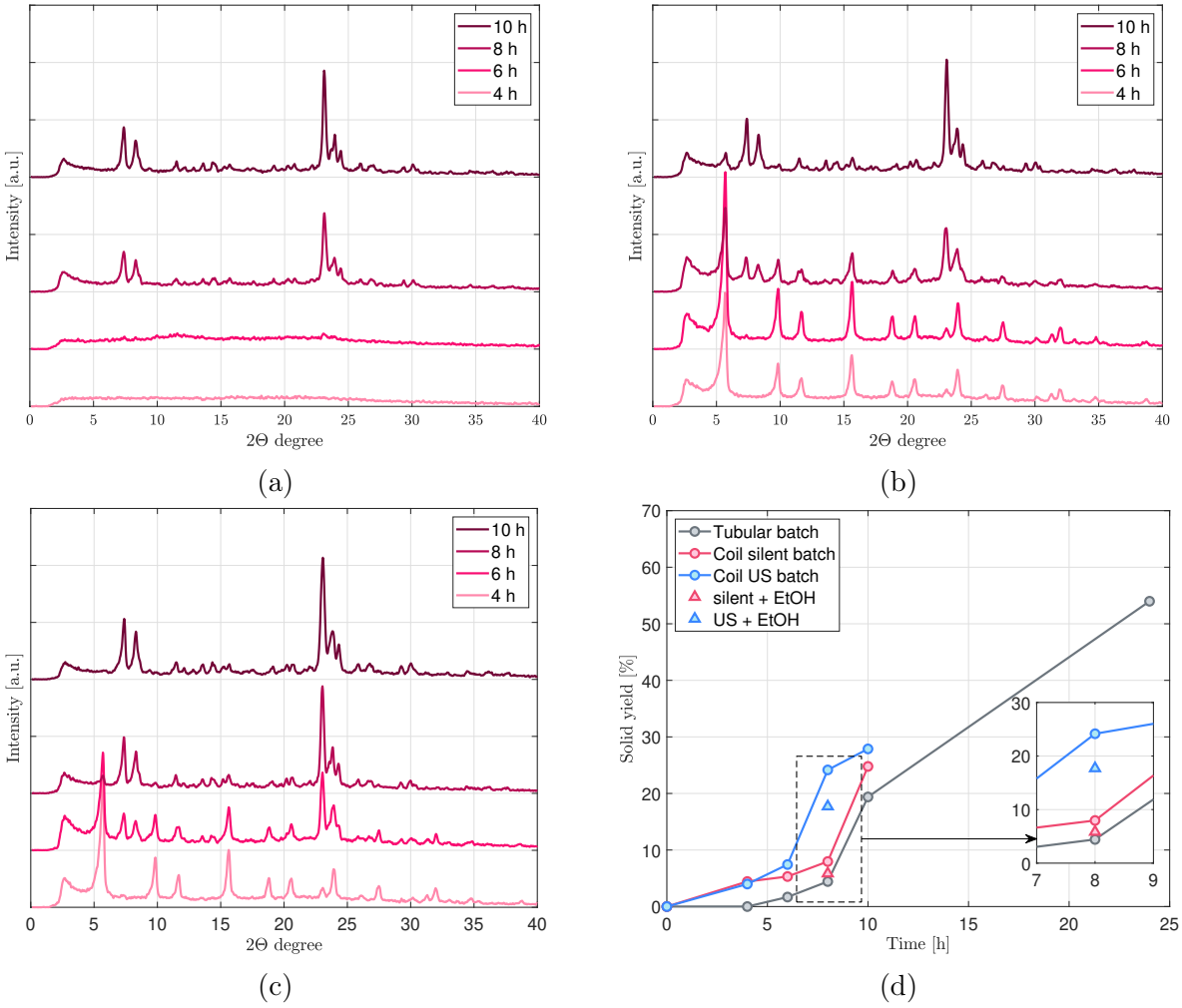

Figure S14: XRD crystallinity pattern evolution over time of FAU-to-MFI IZC at 90 °C in a) tubular batch reactor, silent conditions, b) coiled batch reactor, silent conditions, and c) coiled batch reactor, 240 W ultrasound applied. Figure d) shows the total solid yield of the syntheses at 90 °C with and without 800 mM of EtOH as a radical scavenger.

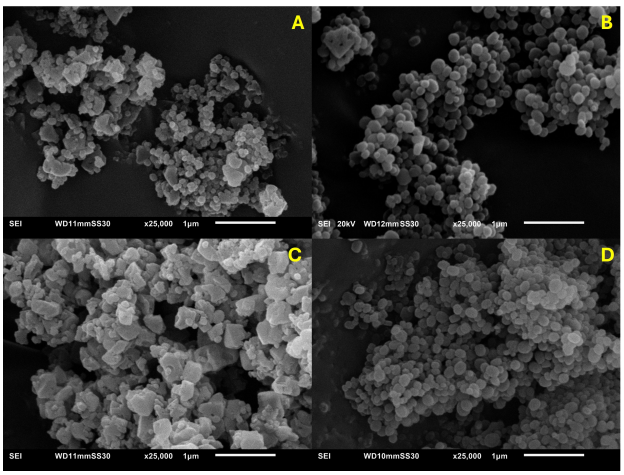

Figure S15: SEM images of 8 h, 90 °C FAU-to-MFI interzeolite conversion in the coiled reactor under different conditions: a) 0 W, 0 mM EtOH; b) 240 W, 0 mM EtOH; C) 0 W, 800 mM EtOH, D) 240 W, 800 mM EtOH.

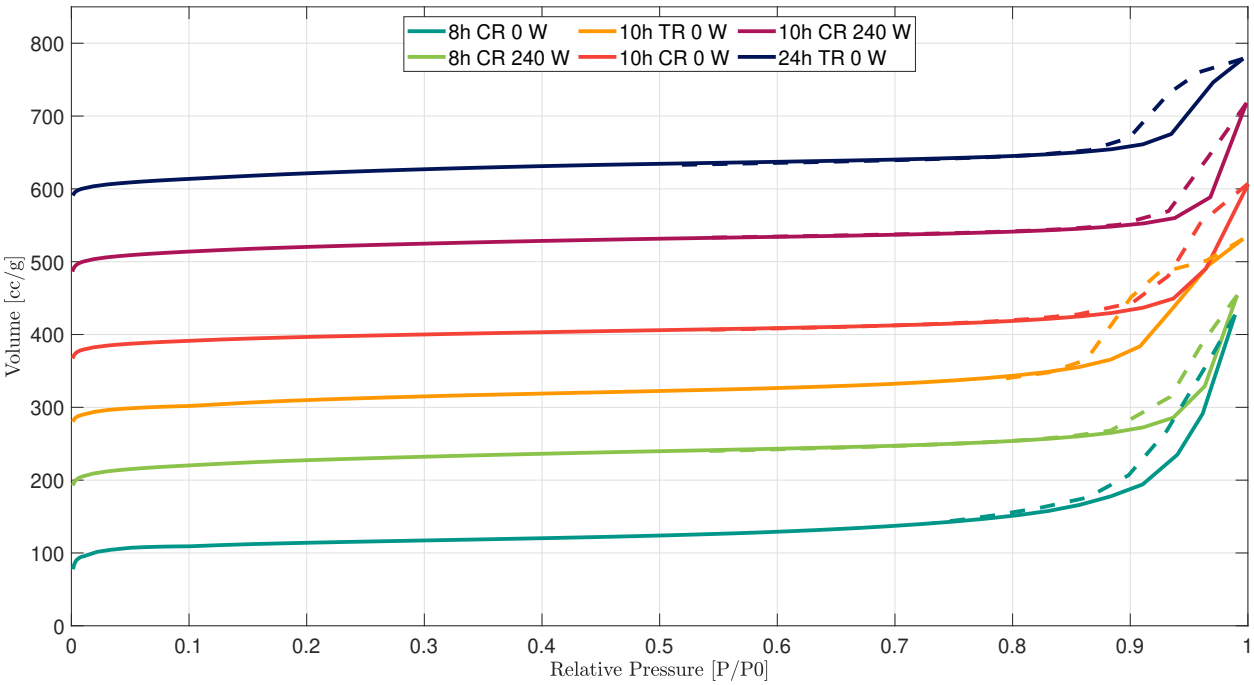

Figure S16: N_2 physisorption isotherms for low temperature FAU to MFI interzeolite conversion in tubular (TR), coiled (CR) reactors, with and without the use of 240 W ultrasound. The curves are plotted with an offset value of 100.

S(V): Crystal size, partial sonication and solid deposition evaluation

Evolution of the crystal mean size over time and its first derivative, *i.e.*, the growth rate, are analysed in Figure S17 for the silent and irradiated case in hydrothermal conditions (160

°C, 6.5 bar), respectively. In the absence of ultrasound, depicted in Figure S17a, particle growth occurs mostly between 30 and 45 min, after which the mean size reaches a plateau. The growth rate curve is narrow and peaks at a higher value compared to the US-assisted synthesis, in Figure S17b. In this case, the growth rate curve has already begun to rise at 20 min residence time, and flattens out only around 100 min. The broader curve reflects the prolonged crystal growth that occurs under ultrasonication, and therefore its final larger mean crystal size compared to the silent case.

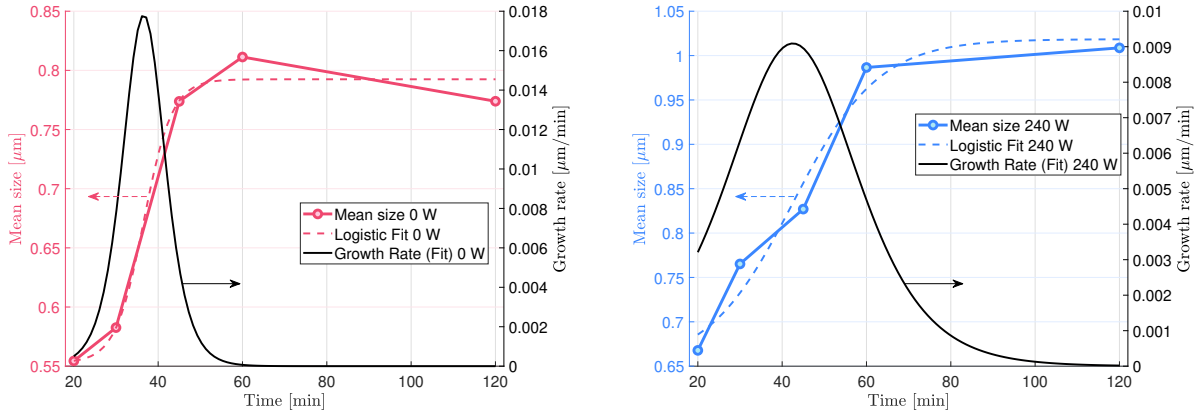

(a) (b)

Figure S17: Evolution over time of the mean crystal size, its logistic regression and the derivative of the fit expressed as growth rate for hydrothermal MFI IZC in the CR a) silent conditions, b) under 240 W ultrasonication.

The PXRD patterns of partial sonication experiments are shown in Figure S18; a direct comparison can be made between ultrasound irradiation in the first part of the synthesis (Figure S18a), versus the second part of the synthesis, until the end of the total 30 min (Figure S18b). The major difference that can be detected is the gradual disappearance of the FAU peak at θ=6° the longer the solution is exposed to ultrasound. However, a difference in this peak's intensity is evident between the silent and irradiated cases; assuming a similar extent of undissolved FAU for both start- and end-of-reaction sonication, and knowing that the amount of product collected is higher for end-of-the-reaction sonication, the intensity of the peak around θ=6° that represents the remainders of the undissolved FAU will be in this case lower, therefore making the differences in crystallinity less clear as compared

to the start-of-reaction sonication case. We note however to be careful with quantitative conclusions from a high-throughput transmission mode XRD measurements.

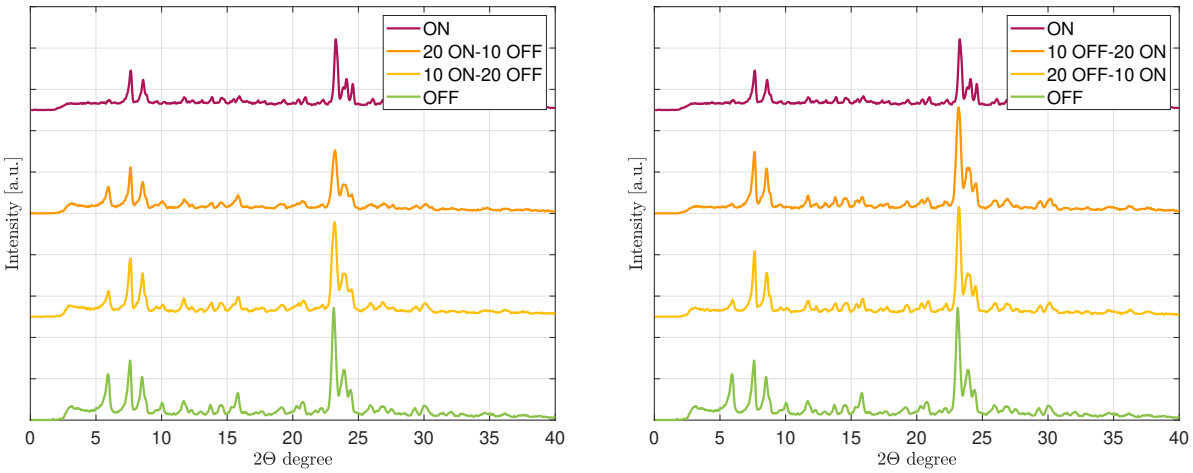

Figure S18: PXRD patterns of partial sonication experiments over a total reaction time of 30 min; a) sonication occurs at the beginning of the synthesis (ON-OFF experiments), versus b) sonication occurs at the end of the synthesis (OFF-ON experiments).

It can be seen in Figure S19a how ultrasound effectively counteracts solid deposition. In the silent case, deposition is uncontrollable, as evident by the very large error bars in the graph, which directly affect the error bars on the solid yield as well. Overall, accounting for the total solids produced in each case (dashed bars), a clear increase in the solid yield can be seen, especially between applying 120 W and 240 W, demonstrating once more the positive effect of ultrasound on IZC kinetics already in the first 30 min of the process. Likewise, by looking at the CSD in Figure S19b, the same conclusion can be drawn.

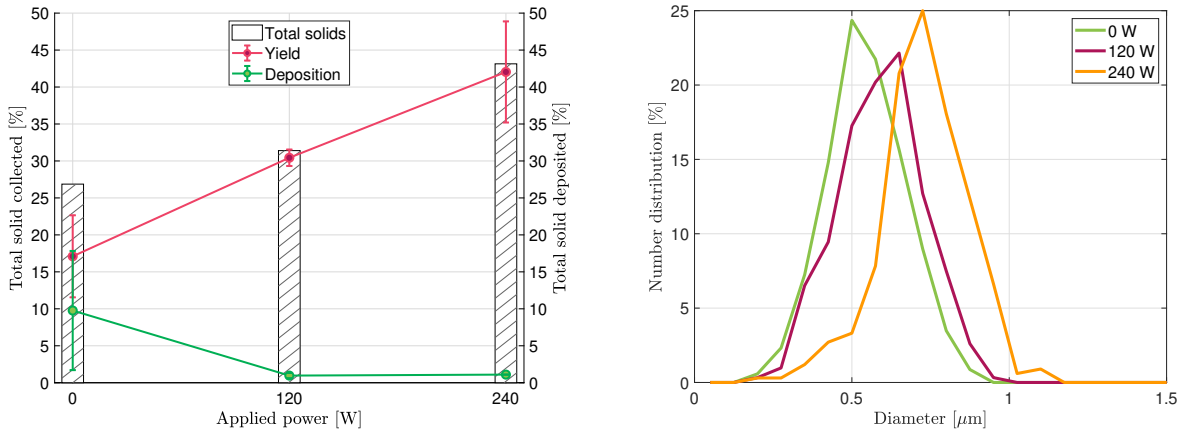

(a) (b)

Figure S19: a) Amount of solids collected from the 30 min synthesis at different net input power (left axis, pink) versus the amount of solids collected during the cleaning process (right axis, green), and the total solids as the sum of the average collection during synthesis and cleaning. b) Number crystal size distribution of MFI at different net input power for 30 min synthesis time.

References

(1) Schneider, C. A.; Rasband, W. S.; Eliceiri, K. W. NIH Image to ImageJ: 25 years of image analysis. *Nat. Methods* **2012**, *9*, 671–675.

(2) IZA Tetrapropylammonium ZSM-5 PXRD reference patterns. `https://europe.iza-structure.org/IZA-SC/pow_plot.php`.

(3) Crislip, J. C.; Vicens, J.; Pham, T.; Zhang, Y.; Tompsett, G.; Teixeira, A. R. Dominance of heat transfer limitations in conventional sol-gel synthesis of LTA revealed by microcrystallization. *J. Flow Chem.* **2022**, *12*, 397–408.

(4) Liu, Z.; Zhu, J.; Wakihara, T.; Okubo, T. Ultrafast synthesis of zeolites: Breakthrough, progress and perspective. *Inorg. Chem. Front.* **2019**, *6*, 14–31.

(5) de Ruiter, R.; Jansen, J. C.; van Bekkum, H. On the incorporation mechanism of B and Al in MFI-type zeolite frameworks. *Zeolites* **1992**, *12*, 56–62.

(6) Montgomery, D. C.; Runger, G. C.; Hubele, N. F. *Engineering Statistics, 5th Edition*; John Wiley & Sons, Incorporated, 2010.

(7) Haw, K.-G.; Gilson, J.-P.; Nesterenko, N.; Akouche, M.; El Siblani, H.; Goupil, J.-M.; Rigaud, B.; Minoux, D.; Dath, J.-P.; Valtchev, V. Supported Embryonic Zeolites and their Use to Process Bulky Molecules. *ACS Catalysis* **2018**, *8*, 8199–8212.

(8) Asswad, E. H.-a.; Dewaele, N.; Nagy, J. B.; Hubert, R. A.; Gabelica, Z.; Paix, N. D. D.; Bruxelles, R. D.; Namur, B.; Applicata, C.; Calabria, U.; Rende, A. Identification of different tetrapropylammonium cations occluded in ZSM-5 zeolite by combined thermal spectroscopy. *Zeolites* **1988**, *8*, 221–227.

(9) Devos, J.; Robijns, S.; Van Goethem, C.; Khalil, I.; Dusselier, M. Interzeolite Conversion and the Role of Aluminum: Toward Generic Principles of Acid Site Genesis and Distributions in ZSM-5 and SSZ-13. *Chem. Mater.* **2021**, *33*, 2516–2531.

(10) Barreto, J. C.; Smith, G. S.; Strobel, N. H.; McQuillin, P. A.; Miller, T. A. Terephthalic acid: A dosimeter for the detection of hydroxyl radicals in vitro. *Life Sci.* **1994**, *56*, 89–96.

(11) Rajamma, D. B.; Anandan, S.; Yusof, N. S. M.; Pollet, B. G.; Ashokkumar, M. Sonochemical dosimetry: A comparative study of Weissler, Fricke and terephthalic acid methods. *Ultrason. Sonochem.* **2021**, *72*, 105413.

(12) Chen, X.; Huang, Z.-H.; Ji, Z.-Y.; Guo, X.-F.; Zhao, L.-M.; Yuan, J.-S. Efficient treatment of pure terephthalic acid wastewater with Na2S2O8 based on thermal activation. *Environmental Technology & Innovation* **2020**, *19*, 100897.

(13) Feng, G.; Cheng, P.; Yan, W.; Boronat, M.; Li, X.; Su, J.-H.; Wang, J.; Li, Y.; Corma, A.; Xu, R.; Yu, J. Accelerated crystallization of zeolites via hydroxyl free radicals. *Science* **2016**, *351*, 1188–1191.

(14) Ding, L.; Hou, Y.; Liu, H.; Peng, J.; Cao, Z.; Zhang, Y.; Wang, B.; Cao, X.; Chang, Y.; Wang, T.; Liu, G. Alcohols as Scavengers for Hydroxyl Radicals in Photocatalytic Systems: Reliable or Not? *ACS ES&T Water* **2023**, *3*, 3534–3543.

(15) Prokešová-Fojtíková, P.; Mintova, S.; Čejka, J.; Žilková, N.; Zukal, A. Porosity of micro/mesoporous composites. *Microporous and Mesoporous Materials* **2006**, *92*, 154–160.